Nonlinear periodic response analysis of mooring cables using harmonic balance method

Chen, Lin; Basu, Biswajit; Nielsen, Søren R.K.

Published in:
Journal of Sound and Vibration

DOI (link to publication from Publisher):
10.1016/j.jsv.2018.09.027

Publication date:
2019

Document Version
Accepted author manuscript, peer reviewed version

Citation for published version (APA):
Chen, L., Basu, B., & Nielsen, S. R. K. (2019). Nonlinear periodic response analysis of mooring cables using harmonic balance method. *Journal of Sound and Vibration*, *438*, 402-418. https://doi.org/10.1016/j.jsv.2018.09.027

Accepted Manuscript

Nonlinear periodic response analysis of mooring cables using harmonic balance method

Lin Chen, Biswajit Basu, Søren R.K. Nielsen

PII: S0022-460X(18)30612-6

DOI: 10.1016/j.jsv.2018.09.027

Reference: YJSVI 14378

To appear in: *Journal of Sound and Vibration*

Received Date: 22 November 2017

Revised Date: 11 July 2018

Accepted Date: 10 September 2018

Nonlinear periodic response analysis of mooring cables using harmonic balance method

Lin Chen[a], Biswajit Basu[a,*], Søren R.K. Nielsen[b]

[a]School of Engineering, Trinity College Dublin, Dublin 2, Ireland
[b]Department of Civil Engineering, Aalborg University, Aalborg 9000, Denmark

Abstract

Mooring cables are critical components of ocean renewable energy systems including offshore floating wind turbines and wave energy converters. Mooring cable dynamics is strongly nonlinear resulting from the geometric effect, hydrodynamic loads and probably seabed interactions. Time-domain methods are commonly used for numerical simulation. This study formulates a nonlinear frequency domain multi-harmonic balance method for efficient analysis of a mooring cable subjected to periodic fairlead motions. The periodic responses are of particular interest to investigate the mooring effect on the platform. In the formulation, the governing equations of the three-dimensional cable motions are spatially discretized using the finite difference method; the nonlinear ordinary differential equations are subsequently transformed into frequency domain by expanding both the structural responses and the nonlinear nodal forces using truncated Fourier series, leading to a set of nonlinear algebraic equations of the Fourier coefficients. The equations are eventually solved using Newton's method where the alternating frequency/time domain method is used to handle the nonlinearity effect. The presented method is then compared to a time-domain method by numerical studies of a mooring cable. The results show that the method is of comparable accuracy as the time-domain method while it is generally more efficient. The proposed method shows promising results even when the cable tension becomes non-positive for a period of time during the cable motion, which is a known ill-posed problem for time-domain methods.

Keywords: Mooring cables; nonlinear dynamics; harmonic balance method; periodic response; alternating frequency/time domain technique.

1. Introduction

Offshore winds and waves are promising renewable energy sources and are receiving intensive research attention recently. Modeling mooring systems is one of the challenging tasks in simulation and design of such floating offshore structures [1, 2]. Several comparison studies have already shown the importance of mooring cable dynamics on floating wind turbines [3–7]. In the last decade, a number of cable models have been explored, validated or coupled with the multi-body dynamics of floating offshore wind turbines and wave energy devices for numerical simulation, including the finite element model [8, 9], the multi-body dynamics model [10], the lumped mass models [11, 12] and the finite difference model [13–17]. A review of the available models and simulation tools of mooring cables can be found in [18, 19]. Presently, mathematical modeling of mooring cables is still a topic area, e.g. a high-order spectral method has been developed by [20, 21] and modeling cables using bar elements in an open-source library has been conducted in [22].

Despite a large number of models available for dynamic analyses of the mooring cables, the understanding of the mooring cable dynamics is still limited. This is due to the complex nonlinearity arising from the geometric effect, hydrodynamic loads and the seabed contact. Besides, for nonlinear analysis, hundreds of degrees of freedom of one

*Corresponding author.
Email addresses: l.chen.tj@gmail.com (Lin Chen), basub@tcd.ie (Biswajit Basu), srkn@civil.aau.dk (Søren R.K. Nielsen)

Nomenclature

$(\bar{\ })$	variables are constant or dependent of cable static solution
$\mathbf{b}_{n-1/2}$	vectorized Fourier coefficients of $\hat{\mathbf{f}}_{n-1/2}$
$\mathbf{c}_k^{(\ )}, \mathbf{s}_k^{(\ )}$	Fourier coefficients of $\mathbf{y}_n$ or $\mathbf{f}_{n-1/2}$, indicated by the superscripts
β	structural damping coefficient
$\mathbf{h}_{n-1/2}, \mathbf{h}_1, \mathbf{h}_N$	residual vector of the resulting nonlinear algebraic equations corresponding to intermediate and boundary nodes
$\mathbf{I}_{(\ )}$	identity matrix with dimension indicated by the subscript
$\mathbf{q}(t)$	vector containing the sine and cosine series
$\mathbf{y}(s,t)$	$= \left[\tilde{\varepsilon}\ u\ v\ w\ \tilde{\phi}\ \tilde{\theta}\right]^{\top}$, vector of nodal variables
$\mathbf{z}_n$	vectorized Fourier coefficients of $\hat{\mathbf{y}}_n$
$\mathcal{F}^-, \mathcal{F}^+$	inverse FFT and FFT operators
$\Delta\mathbf{z}_n$	increment of the Fourier coefficient vector
$(\dot{\ })$	time derivatives
Δs_{n-1}	cable segment length between node $n-1$ and node n
γ	relaxation factor
$\hat{\mathbf{f}}_{n-1/2}$	vectorized $\tilde{\mathbf{f}}_{n-1/2}$ samples in one oscillation period
$\hat{\mathbf{y}}_n$	vectorized $\mathbf{y}_n$ samples in one oscillation period
$\mathbf{M}, \mathbf{K}, \mathbf{f}$	mass and stiffness matrices, and force vector after moving all nonlinear terms to the force vector
$\mathbf{Q}(\omega)$	Fourier series sampled at discrete time points
ω, T_f	characteristic angular frequency and period of the forced fairlead motion
$\otimes$	Kronecker product operator
ϕ, θ	angles
ρ_w	the density of water
$\mathbf{\Theta}, \mathbf{\Theta}_k$	partial differential operator in frequency domain and its block element
$(\tilde{\ })$	variables dependent of cable dynamic solution
υ	an integer to account for subharmonics in Fourier series
$\varepsilon(s,t)$	cable strain
C_{dt}, C_{dn}, C_{db}	drag coefficients in tangential, normal and bi-normal directions of the moving Lagrangian coordinate system
d	cable diameter
e	error
EA	cable axial stiffness
F_{dt}, F_{dn}, F_{db}	drag forces per unit length in the local coordinate
F_X, F_Y, F_Z	fairlead forces
h, l	static/initial cable depth and radius
i, j	indexes
k	index of harmonics in Fourier series
L_0	unstretched cable length
m	cable mass per unit length
m_a	added mass per unit length
N	cable node number
n	cable node index
N_c	number of Fourier coefficients for each unknown
N_h	number of harmonics retained in truncated Fourier expansion
N_t	number of time instances used for discretization the one period
N_y	number of nodal variables
s	arc length coordinate of the unstretched cable
t	time
$u(s,t), v(s,t), w(s,t)$	cable velocity in tangential, normal and bi-normal directions in the moving Lagrangian reference frame
$U(t), V(t), W(t))$	forced fairlead velocities at time t and node N in vertical, horizontal and out-of-plane directions of the fixed reference frame
U_c, V_c, W_c	current velocities in the vertical and horizontal, and out-of-plane directions of the fixed reference coordinate system
$u_r(s,t), v_r(s,t), w_r(s,t)$	relative velocities of the cable with respect to fluid current in the moving Lagrangian reference frame
w_0	submerged cable weight per unit length
w_e	effective cable submerged weight per unit length considering seabed effect

cable need to be considered for accuracy and hence the computational demand is another difficulty. Characterizing the cable dynamics is important for improving the computational efficiency for the coupled analyses, e.g. by model reduction and also for the interpretation of the coupled analysis results. In this context, this study focuses on the research gap of nonlinear responses of a mooring cable subjected to periodic fairlead excitations, which represent an important subset of the cable dynamics and also are important for understanding the nonlinear mooring loads on the structures in the steady state. For understanding the dynamic behavior of submerged cables, linearization methods [23–25] including linearization based frequency domain methods have been used to study towed cable dynamics [26]. The second-order nonlinear dynamics of catenary pipelines/cables have been studied using a perturbation technique based on the finite difference model [27]. However, those methods can only give approximate solutions of the cable responses. In this study, the nonlinear periodic motion is proposed to be solved efficiently and accurately using a multi-Harmonic Balance (multi-HB) method.

The harmonic balance method may date back to [28–30] and it has been widely used as an efficient method for computing periodic and steady-state responses of nonlinear systems and, hence to gain insight into system nonlinear characteristics. Furthermore, the introduction of the Fast Fourier Transform (FFT) and the Alternating Frequency/Time (AFT) technique [31–34] enables the use of multiple (high-order) harmonics and accurate consideration of strong nonlinearity such as friction. With the AFT technique, it has been shown that the Jacobian matrix of the nonlinear algebraic equations resulting from multi-HB analysis can be formulated analytically, even for stiff systems with friction interfaces, which guarantees the computational efficiency. Currently, the multi-HB method is capable of studying the stability and nonlinear normal modes of large nonlinear systems as described in [35, 36]. It has been applied to aerospace structures [37], flexible structures with local nonlinear attachments [38–40], stay cables [41], and nonlinear mechanical systems [42], to name but a few. The single-term harmonic balance has been used for linearizing mooring dynamics by [24, 43, 44]. The multi-HB method, however, has not been applied to submerged cables with hydrodynamic effects so far.

This paper is structured as follows. After this introduction, Section 2 presents the nonlinear hydrodynamics of mooring cables along with a finite difference method for spatial discretization. Section 3 formulates the multi-HB method for mooring cables together with the AFT technique. Numerical studies are presented in Section 4 to demonstrate the effectiveness and advantages of the method by comparison with a time-domain method. A brief conclusion is provided in Section 5.

2. Nonlinear hydrodynamics of mooring cables

The mooring cable under consideration has uniform properties and circular or annular cross-section with the outter diameter d, mass per unit length m, and submerged weight per unit length w_0 when unstretched. A linear strain and tension relationship is considered with EA denoting the axial stiffness. The unstretched cable length is denoted by L_0. The density of water is denoted by ρ_w. The initial cable depth and radius are denoted by h and l respectively, as shown in Fig. 1.

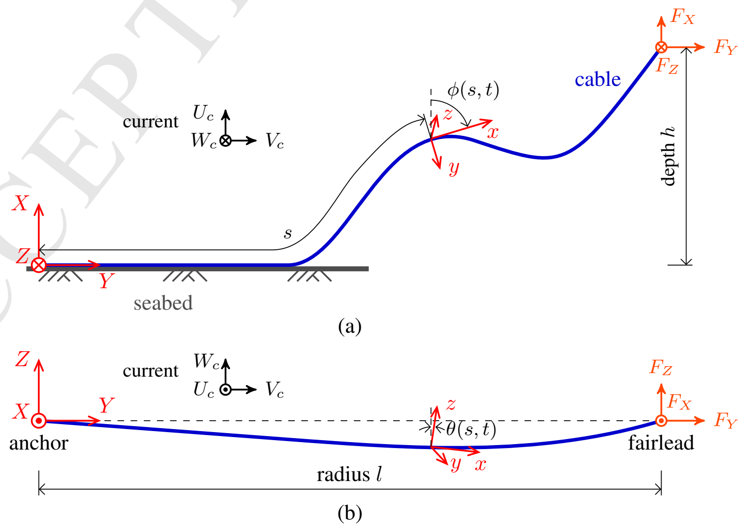

Figure 1: Submerged mooring cable and the coordinate system for describing its motion: (a) front view; (b) top view.

2.1. Governing Equations

The cable model derived in [13, 14] is used here. The bending and torsional stiffnesses are ignored because they are quite small for mooring cables and hence have limited effects on the cable responses. The coordinate systems for describing the three-dimensional mooring configuration and motion are shown in Fig. 1. The origin of the fixed reference frame (X, Y, Z) is located at the cable anchorage on the seabed with $X-Y$ plane as the vertical plane defined by the anchor and the initial cable top end location and the X-axis is pointing upwards. A moving Lagrangian reference frame (x, y, z) is attached to the cable at an arc length s of the unstretched cable measuring from the seabed anchor. The x-axis is aligned with the local tangent direction. The angle between x-axis and X-axis in $X-Y$ plane is denoted by ϕ and the angle between x-axis and Y-axis in $Y-Z$ plane is denoted by θ. The cable curvatures in the $X-Y$ plane and the $Y-Z$ plane are then defined by $\partial\phi/\partial s$ and $\partial\theta/\partial s$ respectively. For the case concerned here where the cable is axisymmetric and the bending and torsion are ignored, the two angles (ϕ, θ) along with s are found to be sufficient to define the cable configuration [13]. The normal and binormal directions (y, z) of the local reference frame are defined correspondingly after the transformation, using the two angles, to align X-axis to the local tangent direction.

Considering a steady current velocity with three components in the fixed reference frame, denoted by U_c, V_c and W_c respectively, from the balance of forces in the Lagrangian reference frame together with the compatibility relations, the partial differential equations (PDEs) governing the cable motion are given as [13]

$$0 = EA\frac{\partial\varepsilon}{\partial s} - m\frac{\partial u}{\partial t} + mv\cos\theta\frac{\partial\phi}{\partial t} - mw\frac{\partial\theta}{\partial t} + EA\beta\frac{\partial\varepsilon}{\partial t} - w_0\cos\phi\cos\theta + F_{dt} \tag{1}$$

$$0 = EA\varepsilon\cos\theta\frac{\partial\phi}{\partial s} - (m+m_a)\frac{\partial v}{\partial t} - m(u\cos\theta + w\sin\theta)\frac{\partial\phi}{\partial t} - C_m\rho_w\frac{\pi d^2}{4}(U_c\cos\phi + V_c\sin\phi)\frac{\partial\phi}{\partial t} + w_0\sin\phi + F_{dn} \tag{2}$$

$$\begin{aligned}0 = &- EA\varepsilon\frac{\partial\theta}{\partial s} - (m+m_a)\frac{\partial w}{\partial t} + mv\sin\theta\frac{\partial\phi}{\partial t} - C_m\rho_w\frac{\pi d^2}{4}(U_c\sin\phi\sin\theta - V_c\cos\phi\sin\theta)\frac{\partial\phi}{\partial t} + mu\frac{\partial\theta}{\partial t}\\ &+ C_m\rho_w\frac{\pi d^2}{4}(U_c\cos\phi\cos\theta + V_c\sin\phi\cos\theta - W_c\sin\theta)\frac{\partial\theta}{\partial t} - w_0\cos\phi\sin\theta + F_{db}\end{aligned} \tag{3}$$

$$0 = \frac{\partial u}{\partial s} - \frac{\partial\varepsilon}{\partial t} + w\frac{\partial\theta}{\partial s} - v\frac{\partial\phi}{\partial s}\cos\theta \tag{4}$$

$$0 = \frac{\partial v}{\partial s} - (1+\varepsilon)\cos\theta\frac{\partial\phi}{\partial t} + \frac{\partial\phi}{\partial s}\cos\theta(u + w\tan\theta) \tag{5}$$

$$0 = \frac{\partial w}{\partial s} + (1+\varepsilon)\frac{\partial\theta}{\partial t} - v\frac{\partial\phi}{\partial s}\sin\theta - \frac{\partial\theta}{\partial s}u \tag{6}$$

where $\varepsilon(s,t)$ = cable strain; $u(s,t)$, $v(s,t)$ and $w(s,t)$ are the tangential, normal, and bi-normal components of cable velocity. The buoyancy effect is included in calculation of the submerged weight per unit length w_0; the Froude-Krylov force, hydrodynamic mass and drag forces are considered using modified Morison's formula [45]. The added mass is calculated by $m_a = C_a\rho_w\pi d^2/4$ with the added mass coefficient denoted by C_a. The inertia coefficient is given as $C_m = 1 + C_a$. A structural damping term is added into Eq. (1) as $\beta EA\partial\varepsilon/\partial t$ assuming proportional damping [12]. The cable velocities relative to the fluid in the Lagrangian reference frame are denoted as $u_r(s,t)$, $v_r(s,t)$ and $w_r(s,t)$, i.e.

$$u_r = u - (U_c\cos\phi\cos\theta + V_c\sin\phi\cos\theta - W_c\sin\theta) \tag{7}$$

$$v_r = v - (-U_c\sin\phi + V_c\cos\phi) \tag{8}$$

$$w_r = w - (U_c\cos\phi\sin\theta + V_c\sin\phi\sin\theta + W_c\cos\theta) \tag{9}$$

The hydrodynamic drag forces are given as

$$F_{dt} = -\frac{1}{2}\rho_w d\pi C_{dt}|u_r|u_r\sqrt{1+\varepsilon} \tag{10}$$

$$F_{dn} = -\frac{1}{2}\rho_w d C_{dn} v_r\sqrt{v_r^2+w_r^2}\sqrt{1+\varepsilon} \tag{11}$$

$$F_{db} = -\frac{1}{2}\rho_w d C_{db} w_r\sqrt{v_r^2+w_r^2}\sqrt{1+\varepsilon} \tag{12}$$

96 where C_{dt}, C_{dn}, and C_{db} are the drag coefficients in tangential, normal and binormal directions.

97 *2.2. Incremental form of the governing equations*

98 For dynamic analysis, the static solution is assumed to be known, which fulfills the static equations that

$$0 = EA\frac{\mathrm{d}\bar{\varepsilon}}{\mathrm{d}s} - w_0\cos\bar{\phi}\cos\bar{\theta} + \bar{F}_{dt} \tag{13}$$

$$0 = EA\bar{\varepsilon}\cos\bar{\theta}\frac{\mathrm{d}\bar{\phi}}{\mathrm{d}s} + w_0\sin\bar{\phi} + \bar{F}_{dn} \tag{14}$$

$$0 = -EA\bar{\varepsilon}\frac{\mathrm{d}\bar{\theta}}{\mathrm{d}s} - w_0\cos\bar{\phi}\sin\bar{\theta} + \bar{F}_{db} \tag{15}$$

99 where $\bar{\varepsilon}, \bar{\phi}$ and $\bar{\theta}$ are the static solutions, and $\bar{F}_{dt}, \bar{F}_{dn}$ and $\bar{F}_{db}$ are hydaulic drag forces when the cable is at rest. The
100 preceding equations can be rewritten as

$$\frac{\mathrm{d}\bar{\varepsilon}}{\mathrm{d}s} = \frac{1}{EA}\left(w_0\cos\bar{\phi}\cos\bar{\theta} - \bar{F}_{dt}\right) \tag{16}$$

$$\frac{\mathrm{d}\bar{\phi}}{\mathrm{d}s} = -\frac{1}{EA\bar{\varepsilon}\cos\bar{\theta}}\left(w_0\sin\bar{\phi} + \bar{F}_{dn}\right) \tag{17}$$

$$\frac{\mathrm{d}\bar{\theta}}{\mathrm{d}s} = -\frac{1}{EA\bar{\varepsilon}}\left(w_0\cos\bar{\phi}\sin\bar{\theta} - \bar{F}_{db}\right) \tag{18}$$

101 Correspondingly, the relative velocity of the static cable with respect to water is defined as

$$\begin{aligned}
\bar{u}_r &= -U_c\cos\bar{\phi}\cos\bar{\theta} - V_c\sin\bar{\phi}\cos\bar{\theta} + W_c\sin\bar{\theta}\\
\bar{v}_r &= U_c\sin\bar{\phi} - V_c\cos\bar{\phi}\\
\bar{w}_r &= -U_c\cos\bar{\phi}\sin\bar{\theta} - V_c\sin\bar{\phi}\sin\bar{\theta} - W_c\cos\bar{\theta}
\end{aligned}$$

102 The cable state can be expressed as the summation of its static and dynamic components as

$$\varepsilon(s,t) = \bar{\varepsilon}(s) + \tilde{\varepsilon}(s,t), \phi(s,t) = \bar{\phi}(s) + \tilde{\phi}(s,t), \theta(s,t) = \bar{\theta}(s) + \tilde{\theta}(s,t) \tag{19}$$

103 and hence the governing equations are rewritten in an incremental form as

$$0 = EA\frac{\partial(\bar{\varepsilon}+\tilde{\varepsilon})}{\partial s} - m\frac{\partial u}{\partial t} + mv\cos\theta\frac{\partial\tilde{\phi}}{\partial t} - mw\frac{\partial\tilde{\theta}}{\partial t} + EA\beta\frac{\partial\tilde{\varepsilon}}{\partial t} - w_0\cos\phi\cos\theta + F_{dt} \tag{20}$$

$$\begin{aligned} 0 =& EA(\bar{\varepsilon}+\tilde{\varepsilon})\cos\theta\frac{\partial(\bar{\phi}+\tilde{\phi})}{\partial s} - (m+m_a)\frac{\partial v}{\partial t} \\ &- m\left[u\cos\theta + w\sin\theta\right]\frac{\partial\tilde{\phi}}{\partial t} - C_m\rho_w\frac{\pi d^2}{4}\left(U_c\cos\phi + V_c\sin\phi\right)\frac{\partial\tilde{\phi}}{\partial t} + w_0\sin\phi + F_{dn} \end{aligned} \tag{21}$$

$$\begin{aligned} 0 =& -EA\varepsilon\frac{\partial(\bar{\theta}+\tilde{\theta})}{\partial s} - (m+m_a)\frac{\partial w}{\partial t} + mv\sin\theta\frac{\partial\tilde{\phi}}{\partial t} - C_m\rho_w\frac{\pi d^2}{4}\left(U_c\sin\phi\sin\theta - V_c\cos\phi\sin\theta\right)\frac{\partial\tilde{\phi}}{\partial t} \\ &+ mu\frac{\partial\tilde{\theta}}{\partial t} + C_m\rho_w\frac{\pi d^2}{4}\left(U_c\cos\phi\cos\theta + V_c\sin\phi\cos\theta - W_c\sin\theta\right)\frac{\partial\tilde{\theta}}{\partial t} - w_0\cos\phi\sin\theta + F_{db} \end{aligned} \tag{22}$$

$$0 = \frac{\partial u}{\partial s} - \frac{\partial\tilde{\varepsilon}}{\partial t} + w\frac{\partial(\bar{\theta}+\tilde{\theta})}{\partial s} - v\frac{\partial(\bar{\phi}+\tilde{\phi})}{\partial s}\cos(\bar{\theta}+\tilde{\theta}) \tag{23}$$

$$0 = \frac{\partial v}{\partial s} - (1+\bar{\varepsilon}+\tilde{\varepsilon})\cos(\theta+\tilde{\theta})\frac{\partial\tilde{\phi}}{\partial t} + \frac{\partial(\bar{\phi}+\tilde{\phi})}{\partial s}\cos(\bar{\theta}+\tilde{\theta})\left[u + w\tan(\bar{\theta}+\tilde{\theta})\right] \tag{24}$$

$$0 = \frac{\partial w}{\partial s} + (1+\bar{\varepsilon}+\tilde{\varepsilon})\frac{\partial\tilde{\theta}}{\partial t} - v\frac{\partial(\bar{\phi}+\tilde{\phi})}{\partial s}\sin(\bar{\theta}+\tilde{\theta}) - \frac{\partial(\bar{\theta}+\tilde{\theta})}{\partial s}u \tag{25}$$

2.3. *Equations in matrix form*

The PDEs using the incremental formulation can be written in matrix form as

$$\mathbf{M}(\mathbf{y})\frac{\partial\mathbf{y}}{\partial t} + \mathbf{K}(\mathbf{y})\frac{\partial\mathbf{y}}{\partial s} + \mathbf{f}(\mathbf{y}) = 0 \tag{26}$$

where the nodal state vector is $\mathbf{y}(s,t) = [\tilde{\varepsilon}, u, v, w, \tilde{\phi}, \tilde{\theta}]^\top$, $\mathbf{M}$ and $\mathbf{K}$ are mass and stiffness matrices, and $\mathbf{f}$ is the nodal force vector. They are given as below

$$\mathbf{K} = \begin{bmatrix} EA & 0 & 0 & 0 & 0 & 0 \\ 0 & 0 & 0 & 0 & EA\varepsilon\cos\theta & 0 \\ 0 & 0 & 0 & 0 & 0 & -EA\varepsilon \\ 0 & 1 & 0 & 0 & -v\cos\theta & w \\ 0 & 0 & 1 & 0 & u\cos\theta + w\sin\theta & 0 \\ 0 & 0 & 0 & 1 & -v\sin\theta & -u \end{bmatrix} \tag{27}$$

$$\mathbf{M} = \begin{bmatrix} EA\beta & -m & 0 & 0 & mv\cos\theta & -mw \\ 0 & 0 & -(m+m_a) & 0 & M_{2,5} & 0 \\ 0 & 0 & 0 & -(m+m_a) & M_{3,5} & M_{3,6} \\ -1 & 0 & 0 & 0 & 0 & 0 \\ 0 & 0 & 0 & 0 & M_{5,5} & 0 \\ 0 & 0 & 0 & 0 & 0 & 1+\varepsilon \end{bmatrix} \tag{28}$$

where

$$\begin{aligned} M_{2,5} &= -m(w\sin\theta + u\cos\theta) - C_m\rho_w\frac{\pi d^2}{4}(U_c\cos\phi + V_c\sin\phi) \\ M_{3,5} &= mv\sin\theta - C_m\rho_w\frac{\pi d^2}{4}(U_c\sin\phi\sin\theta - V_c\cos\phi\sin\theta) \\ M_{3,6} &= mu + C_m\rho_w\frac{\pi d^2}{4}(U_c\cos\phi\cos\theta + V_c\sin\phi\cos\theta - W_c\sin\theta) \\ M_{5,5} &= -(1+\varepsilon)\cos\theta \end{aligned}$$

and the force vector $\mathbf{f} = [f_1 \;\; f_2 \;\; f_3 \;\; f_4 \;\; f_5 \;\; f_6]^\top$

$$
\begin{aligned}
f_1 =& -w_0 \cos\phi \cos\theta + F_{dt} + EA\frac{\mathrm{d}\bar{\varepsilon}}{\mathrm{d}s} && (29)\\
f_2 =& w_0 \sin\phi + F_{dn} - EA\varepsilon \cos\theta \frac{\mathrm{d}\bar{\phi}}{\mathrm{d}s} && (30)\\
f_3 =& -w_0 \cos\phi \sin\theta + F_{db} - EA\varepsilon \frac{\mathrm{d}\bar{\theta}}{\mathrm{d}s} && (31)\\
f_4 =& -v \cos\theta \frac{\mathrm{d}\bar{\phi}}{\mathrm{d}s} + w\frac{\mathrm{d}\bar{\theta}}{\mathrm{d}s} && (32)\\
f_5 =& (u\cos\theta + w\sin\theta)\frac{\mathrm{d}\bar{\phi}}{\mathrm{d}s} && (33)\\
f_6 =& -v \sin\theta \frac{\mathrm{d}\bar{\phi}}{\mathrm{d}s} + u\frac{\mathrm{d}\bar{\theta}}{\mathrm{d}s} && (34)
\end{aligned}
$$

Noting that $\mathbf{M}, \mathbf{K}$ and $\mathbf{f}$ depend on $\mathbf{y}$, for the convenience of formulating the harmonic balance analysis, the governing equations are rewritten by collecting all the $\mathbf{y}$-dependent terms in the nodal force vector such that

$$
\bar{\mathbf{M}}\frac{\partial \mathbf{y}}{\partial t} + \bar{\mathbf{K}}\frac{\partial \mathbf{y}}{\partial s} + \tilde{\mathbf{M}}(\mathbf{y})\frac{\partial \mathbf{y}}{\partial t} + \tilde{\mathbf{K}}(\mathbf{y})\frac{\partial \mathbf{y}}{\partial s} + \mathbf{f}(\mathbf{y}) = \mathbf{0} \tag{35}
$$

The mass and stiffness matrices, and force vector thus become

$$
\bar{\mathbf{M}} = \begin{bmatrix}
EA\beta & -m & 0 & 0 & 0 & 0\\
0 & 0 & -m - m_a & 0 & 0 & 0\\
0 & 0 & 0 & -m - m_a & 0 & 0\\
-1 & 0 & 0 & 0 & 0 & 0\\
0 & 0 & 0 & 0 & -(1+\bar{\varepsilon})\cos\bar{\theta} & 0\\
0 & 0 & 0 & 0 & 0 & 1+\bar{\varepsilon}
\end{bmatrix} \tag{36}
$$

$$
\bar{\mathbf{K}} = \begin{bmatrix}
EA & 0 & 0 & 0 & 0 & 0\\
0 & 0 & 0 & 0 & EA\bar{\varepsilon}\cos\bar{\theta} & 0\\
0 & 0 & 0 & 0 & 0 & -EA\bar{\varepsilon}\\
0 & 1 & 0 & 0 & 0 & 0\\
0 & 0 & 1 & 0 & 0 & 0\\
0 & 0 & 0 & 1 & 0 & 0
\end{bmatrix} \tag{37}
$$

and

$$
\tilde{\mathbf{M}} = \begin{bmatrix}
0 & 0 & 0 & 0 & mv\cos\theta & -mw\\
0 & 0 & 0 & 0 & M_{2,5} & 0\\
0 & 0 & 0 & 0 & M_{3,5} & M_{3,6}\\
0 & 0 & 0 & 0 & 0 & 0\\
0 & 0 & 0 & 0 & M_{5,5} + (1+\bar{\varepsilon})\cos\bar{\theta} & 0\\
0 & 0 & 0 & 0 & 0 & \tilde{\varepsilon}
\end{bmatrix}, \quad
\tilde{\mathbf{K}} = \begin{bmatrix}
0 & 0 & 0 & 0 & 0 & 0\\
0 & 0 & 0 & 0 & EA\varepsilon\cos\theta - EA\bar{\varepsilon}\cos\bar{\theta} & 0\\
0 & 0 & 0 & 0 & 0 & -EA\tilde{\varepsilon}\\
0 & 0 & 0 & 0 & -v\cos\theta & w\\
0 & 0 & 0 & 0 & u\cos\theta + w\sin\theta & 0\\
0 & 0 & 0 & 0 & -v\sin\theta & -u
\end{bmatrix} \tag{38}
$$

As in [13–16], Eq. (26) along with boundary conditions can be discritized in both time and space using the finite difference method and then solved using the relaxation method [46]. For formulating the multi-HB analysis, the equation is only spatially discretized using the finite difference method.

2.4. Spatial discretization

For spatial discretization, the spatial derivatives Eq. (26) are replaced by the central differences [13, 16]. Let the cable be discretized into $N - 1$ segments with N nodal points in total along the cable length. The first node is at the seabed origin and the Nth node is at the cable top end. Hence, a set of $N-1$ matrix equations (one equation per half grid) can be obtained as

$$\begin{bmatrix}\bar{\mathbf{M}}_{n-1} & \bar{\mathbf{M}}_n\end{bmatrix}\begin{Bmatrix}\dot{\mathbf{y}}_{n-1}\\ \dot{\mathbf{y}}_n\end{Bmatrix} + \frac{1}{\Delta s_{n-1}}\begin{bmatrix}-\bar{\mathbf{K}}_{n-1}-\bar{\mathbf{K}}_n & \bar{\mathbf{K}}_{n-1}+\bar{\mathbf{K}}_n\end{bmatrix}\begin{Bmatrix}\mathbf{y}_{n-1}\\ \mathbf{y}_n\end{Bmatrix} + \begin{bmatrix}\tilde{\mathbf{M}}_{n-1} & \tilde{\mathbf{M}}_n\end{bmatrix}\begin{Bmatrix}\dot{\mathbf{y}}_{n-1}\\ \dot{\mathbf{y}}_n\end{Bmatrix} + \frac{1}{\Delta s_{n-1}}\begin{bmatrix}-\tilde{\mathbf{K}}_{n-1}-\tilde{\mathbf{K}}_n & \tilde{\mathbf{K}}_{n-1}+\tilde{\mathbf{K}}_n\end{bmatrix}\begin{Bmatrix}\mathbf{y}_{n-1}\\ \mathbf{y}_n\end{Bmatrix} + \mathbf{f}_{n-1} + \mathbf{f}_n = \mathbf{0} \tag{39}$$

which is further written as

$$\begin{bmatrix}\bar{\mathbf{M}}_{n-1} & \bar{\mathbf{M}}_n\end{bmatrix}\begin{Bmatrix}\dot{\mathbf{y}}_{n-1}\\ \dot{\mathbf{y}}_n\end{Bmatrix} + \begin{bmatrix}-\bar{\mathbf{K}}_{n-1/2} & \bar{\mathbf{K}}_{n-1/2}\end{bmatrix}\begin{Bmatrix}\mathbf{y}_{n-1}\\ \mathbf{y}_n\end{Bmatrix} + \tilde{\mathbf{f}}_{n-1/2} = \mathbf{0} \tag{40}$$

with

$$\begin{aligned}\bar{\mathbf{K}}_{n-1/2} &= \left(\bar{\mathbf{K}}_{n-1} + \bar{\mathbf{K}}_n\right)/\Delta s_{n-1},\\ \tilde{\mathbf{f}}_{n-1/2} &= \begin{bmatrix}\tilde{\mathbf{M}}_{n-1} & \tilde{\mathbf{M}}_n\end{bmatrix}\begin{Bmatrix}\dot{\mathbf{y}}_{n-1}\\ \dot{\mathbf{y}}_n\end{Bmatrix} + \frac{1}{\Delta s_{n-1}}\begin{bmatrix}-\tilde{\mathbf{K}}_{n-1}-\tilde{\mathbf{K}}_n & \tilde{\mathbf{K}}_{n-1}+\tilde{\mathbf{K}}_n\end{bmatrix}\begin{Bmatrix}\mathbf{y}_{n-1}\\ \mathbf{y}_n\end{Bmatrix} + \mathbf{f}_{n-1} + \mathbf{f}_n\end{aligned} \tag{41}$$

2.5. Boundary conditions

The cable is often fixed at the seabed anchor such that the velocity at the first node is constantly zero

$$u_1 = 0, v_1 = 0, w_1 = 0 \tag{42}$$

On the other hand, the fairlead is subjected to excitations resulting from platform motion. Let the excitation velocity be represented by its three components in the fixed cable coordinate system, i.e. $U(t)$, $V(t)$ and $W(t)$ respectively. Hence, the boundary equations at the fairlead node are given at time t as

$$0 = u_N \cos\phi_N \cos\theta_N - v_N \sin\phi_N + w_N \cos\phi_N \sin\theta_N - U(t) \tag{43}$$

$$0 = u_N \sin\phi_N \cos\theta_N + v_N \cos\phi_N + w_N \sin\phi_N \sin\theta_N - V(t) \tag{44}$$

$$0 = -u_N \sin\theta_N + w_N \cos\theta_N - W(t) \tag{45}$$

Correspondingly the cable tension at the fairlead has three components in the fixed cable coordinate system, as illustrated in Fig. 1, given as

$$F_X(t) = EA\varepsilon_N \cos\phi_N \cos\theta_N \tag{46}$$

$$F_Y(t) = EA\varepsilon_N \sin\phi_N \cos\theta_N \tag{47}$$

$$F_Z(t) = -EA\varepsilon_N \sin\theta_N \tag{48}$$

In cases where the fairlead force is known, the preceding three equations are the boundary conditions at the fairlead. This is usually the case for static analysis.

The mooring cable usually lies partly grounded on the seabed to avoid the lift force to the anchor. For considering the cable-seabed contact effect, the method proposed in [15] is adopted herein. Flat seabed is considered and it is modeled as elastic spring with stiffness k_{sb} which provides a vertical support force when the cable is grounded. This can be easily accounted for by modifying the effective submerged cable weight. In other words, the effective weight per unit length at node n is given as $w_e^n = w_0 + k_{sb}X(s_n)$ and $0 \le w_e^n \le w_0$ for static problem. In solving the PDEs using iterative method, to consider the seabed effect, w_0 in Eqs. (29-34) is replaced by w_e^n which is evaluated based on the cable nodal position obtained in the previous iteration step. After solving the equations in the Lagrangian coordinate system, the cable nodal displacement and position can be integrated node by node from the seabed anchor using s, ϕ and θ [13, 15].

3. Multi-harmonic balance analysis

The nonlinear ordinary equation (39) can also be solved in time domain by replacing the time derivatives using finite differences [16]. However, the time domain method may be subjected to numerical stability issues and to obtain the steady-state responses and a long time simulation may be required to arrive the steady state. This section therefore formulates the multi-HB method for efficiently solving the cable responses when it is subjected to periodic fairlead excitations.

3.1. Governing equations in frequency domain

Considering the cable subjected to a periodic excitation with a period T_f and the corresponding characteristic angular frequency $\omega = 2\pi/T_f$ at its fairlead, the periodic cable response $\mathbf{y}_n$ is pursued herein and hence the nodal force $\mathbf{f}_n$ is also periodic. Therefore, they can be approximated using truncated Fourier series as follows,

$$\mathbf{y}_n(t) \approx \frac{\mathbf{c}_0^{y_n}}{\sqrt{2}} + \sum_{k=1}^{N_h}\left(\mathbf{s}_k^{y_n} \sin\frac{k\omega t}{\upsilon} + \mathbf{c}_k^{y_n} \cos\frac{k\omega t}{\upsilon}\right) \tag{49}$$

$$\tilde{\mathbf{f}}_{n-1/2}(t) \approx \frac{\mathbf{c}_0^{f_{n-1/2}}}{\sqrt{2}} + \sum_{k=1}^{N_h}\left(\mathbf{s}_k^{f_{n-1/2}} \sin\frac{k\omega t}{\upsilon} + \mathbf{c}_k^{f_{n-1/2}} \cos\frac{k\omega t}{\upsilon}\right) \tag{50}$$

in which the index k represents the kth harmonic component and N_h = the number of harmonics retained. Noting that generally the constant terms need to be retained since the presence of the current may induce constant drift of the solution. The total number of coefficient for each degree of freedom is denoted by $N_c = 2N_h + 1$ for general cases and $N_c = 2N_h$ if the constant term is omitted. The integer υ accounts for subharmonics of the excitation frequency ω. The coefficients $\mathbf{c}_k^{(\,)}$ and $\mathbf{s}_k^{(\,)}$ can be reshaped to $N_cN_y \times 1$ vectors as

$$\mathbf{z}_n = \begin{bmatrix} c_0^{y_{n,1}} & s_1^{y_{n,1}} & c_1^{y_{n,1}} & \cdots & s_{N_h}^{y_{n,1}} & c_{N_h}^{y_{n,1}} & \cdots & s_{N_h}^{y_{n,N_y}} & c_{N_h}^{y_{n,N_y}} \end{bmatrix}^\top \tag{51}$$

$$\mathbf{b}_{n-1/2} = \begin{bmatrix} c_0^{f_{n-1/2,1}} & s_1^{f_{n-1/2,1}} & c_1^{f_{n-1/2,1}} & \cdots & s_{N_h}^{f_{n-1/2,1}} & c_{N_h}^{f_{n-1/2,1}} & \cdots & s_{N_h}^{f_{n-1/2,N_y}} & c_{N_h}^{f_{n-1/2,N_y}} \end{bmatrix}^\top \tag{52}$$

where N_y denotes the number of variables at each node, i.e. $N_y = 6$ here. Note that the coefficient arrangements here are different from [47] for the convenience of using relaxation method in the subsequent solving procedure [46]. Then the nodal response and force can be recast into a compact form as

$$\mathbf{y}_n(t) = \left[\mathbf{I}_{N_y} \otimes \mathbf{q}(t)\right]\mathbf{z}_n \tag{53}$$

$$\mathbf{f}_{n-1/2}(t) = \left[\mathbf{I}_{N_y} \otimes \mathbf{q}(t)\right]\mathbf{b}_{n-1/2} \tag{54}$$

where $\otimes$ stands for an operation on two matrices which gives another matrix that is formed by multiplying the second matrix by each element of the first matrix (known as Kronecker product of two matrices, see Appendix A for an example). The matrix $\mathbf{I}_{N_y}$ is an identity matrix of size $N_y \times N_y$, and $\mathbf{q}(t)$ is a row vector containing the sine and cosine series

$$\mathbf{q}(t) = \begin{bmatrix} \frac{1}{\sqrt{2}} & \sin\frac{\omega t}{\upsilon} & \cos\frac{\omega t}{\upsilon} & \cdots & \sin\frac{k\omega t}{\upsilon} & \cos\frac{k\omega t}{\upsilon} & \cdots & \sin\frac{N_h\omega t}{\upsilon} & \cos\frac{N_h\omega t}{\upsilon} \end{bmatrix} \tag{55}$$

From Eq. (53), one obtains

$$\dot{\mathbf{y}}_n(t) = \left[\mathbf{I}_{N_y} \otimes \dot{\mathbf{q}}(t)\right]\mathbf{z}_n = \left\{\mathbf{I}_{N_y} \otimes [\mathbf{q}(t)\boldsymbol{\Theta}]\right\}\mathbf{z}_n \tag{56}$$

in which the matrix $\boldsymbol{\Theta}$ is given as

$$\boldsymbol{\Theta} = \begin{bmatrix} \boldsymbol{\Theta}_1 & & & & \\ & \ddots & & & \\ & & \boldsymbol{\Theta}_k & & \\ & & & \ddots & \\ & & & & \boldsymbol{\Theta}_{N_h} \end{bmatrix} \tag{57}$$

with block entries that

$$\mathbf{\Theta}_k = \begin{bmatrix} 0 & -k\omega/\upsilon \\ k\omega/\upsilon & 0 \end{bmatrix} \tag{58}$$

Substituting expressions (53,56) into Eq. (39), one obtains

$$\begin{bmatrix}\bar{\mathbf{M}}_{n-1} & \bar{\mathbf{M}}_n\end{bmatrix}\left\{\mathbf{I}_{N_y}\otimes[\mathbf{q}(t)\mathbf{\Theta}]\right\}\left\{\begin{array}{c}\mathbf{z}_{n-1}\\ \mathbf{z}_n\end{array}\right\}+\begin{bmatrix}-\bar{\mathbf{K}}_{n-1/2} & \bar{\mathbf{K}}_{n-1/2}\end{bmatrix}\mathbf{I}_{N_y}\otimes\mathbf{q}(t)\left\{\begin{array}{c}\mathbf{z}_{n-1}\\ \mathbf{z}_n\end{array}\right\}+\begin{bmatrix}\mathbf{I}_{N_y}\otimes\mathbf{q}(t)\end{bmatrix}\mathbf{b}_{n-1/2}=\mathbf{0}_{N_y\times 1} \tag{59}$$

where $\mathbf{0}_{N_y\times 1}$ represents a vector of size N_y containing zeros. The preceding equation can be further simplified as

$$\left\{\begin{bmatrix}\bar{\mathbf{M}}_{n-1} & \bar{\mathbf{M}}_n\end{bmatrix}\otimes[\mathbf{q}(t)\mathbf{\Theta}]\right\}\left\{\begin{array}{c}\mathbf{z}_{n-1}\\ \mathbf{z}_n\end{array}\right\}+\left\{\begin{bmatrix}-\bar{\mathbf{K}}_{n-1/2} & \bar{\mathbf{K}}_{n-1/2}\end{bmatrix}\otimes\mathbf{q}(t)\right\}\left\{\begin{array}{c}\mathbf{z}_{n-1}\\ \mathbf{z}_n\end{array}\right\}+\begin{bmatrix}\mathbf{I}_{N_y}\otimes\mathbf{q}(t)\end{bmatrix}\mathbf{b}_{n-1/2}=\mathbf{0}_{N_y\times 1} \tag{60}$$

To eliminate the time dependency of the preceding equation, a Galerkin procedure projects the preceding equation on the orthogonal trigonometric basis of $\mathbf{q}(t)$, namely

$$\begin{aligned}&\left\{\begin{bmatrix}\bar{\mathbf{M}}_{n-1} & \bar{\mathbf{M}}_n\end{bmatrix}\otimes\left[\frac{2}{T_f}\int_0^{T_f}\mathbf{q}^\top(t)\mathbf{q}(t)\mathrm{d}t\mathbf{\Theta}\right]+\begin{bmatrix}-\bar{\mathbf{K}}_{n-1/2} & \bar{\mathbf{K}}_{n-1/2}\end{bmatrix}\otimes\left[\frac{2}{T_f}\int_0^{T_f}\mathbf{q}^\top(t)\mathbf{q}(t)\mathrm{d}t\right]\right\}\left\{\begin{array}{c}\mathbf{z}_{n-1}\\ \mathbf{z}_n\end{array}\right\}\\ &\qquad+\left\{\mathbf{I}_{N_y}\otimes\left[\frac{2}{T_f}\int_0^{T_f}\mathbf{q}^\top(t)\mathbf{q}(t)\mathrm{d}t\right]\right\}\mathbf{b}_{n-1/2}=\mathbf{0}_{N_y\times 1}\end{aligned} \tag{61}$$

Note that

$$\frac{2}{T_f}\int_0^{T_f}\mathbf{q}^\top(t)\mathbf{q}(t)\mathrm{d}t=\mathbf{I}_{N_c}$$

The governing equations are eventually expressed in frequency domain as

$$\left\{\begin{bmatrix}\bar{\mathbf{M}}_{n-1} & \bar{\mathbf{M}}_n\end{bmatrix}\otimes\mathbf{\Theta}+\begin{bmatrix}-\bar{\mathbf{K}}_{n-1/2} & \bar{\mathbf{K}}_{n-1/2}\end{bmatrix}\otimes\mathbf{I}_{N_c}\right\}\left\{\begin{array}{c}\mathbf{z}_{n-1}\\ \mathbf{z}_n\end{array}\right\}+\mathbf{b}_{n-1/2}=\mathbf{0}_{N_cN_y\times 1} \tag{62}$$

The the left-hand side of the preceding equation is defined as the residual, i.e.

$$\mathbf{h}_{n-1/2}=\begin{bmatrix}\bar{\mathbf{M}}_{n-1}\otimes\mathbf{\Theta}-\bar{\mathbf{K}}_{n-1/2}\otimes\mathbf{I}_{N_c} & \bar{\mathbf{M}}_n\otimes\mathbf{\Theta}+\bar{\mathbf{K}}_{n-1/2}\otimes\mathbf{I}_{N_c}\end{bmatrix}\left\{\begin{array}{c}\mathbf{z}_{n-1}\\ \mathbf{z}_n\end{array}\right\}+\mathbf{b}_{n-1/2} \tag{63}$$

for each intermediate node $1 < n \leq N$. Similarly, for the boundary nodes, it reads

$$\mathbf{h}_1=\mathbf{b}_1,\quad \mathbf{h}_N=\mathbf{b}_N \tag{64}$$

For implementation of multi-HB method, it is crucial to determine $\mathbf{b}_n$ and also the Jacobian matrix for gradient based correction of the solution. The AFT method is applied [32], as detailed in the following subsection.

3.2. AFT technique for handling nonlinearity

The expressions for the nonlinear nodal forces as expressed in Eq. (29-34) are difficult to be analytically transformed into frequency domain to obtain the coefficients in the Fourier series. The AFT technique offers a convenient procedure as

$$\mathbf{z}_n,\mathbf{z}_{n-1}\xrightarrow{\mathcal{F}^-}\mathbf{y}_n,\mathbf{y}_{n-1},\dot{\mathbf{y}}_n,\dot{\mathbf{y}}_{n-1}\rightarrow\tilde{\mathbf{f}}_{n-1/2}\xrightarrow{\mathcal{F}^+}\mathbf{b}_{n-1/2} \tag{65}$$

where $\mathcal{F}^-$ denotes the inverse FFT operator and correspondingly the FFT operator is denoted by $\mathcal{F}^+$. In other words, in each iteration step, the nonlinear nodal force is obtained by evaluating Eq. (29-34) in time domain, using time series of the nodal state which are transformed from $\mathbf{z}_n$ and $\mathbf{z}_{n-1}$ using inverse FFT, and further the nodal force time series are transformed into frequency domain for $\mathbf{b}_n$ and $\mathbf{b}_{n-1}$ via FFT.

Let the time period be discretized by N_t equally distributed sampling points in the FFT. One can define vectors $\hat{\mathbf{y}}$ and $\hat{\mathbf{f}}$ containing the concatenated $N_t \cdot N_y$ time samples of the nodal states and the forces, respectively. For the nth node, one thus obtains

$$\hat{\mathbf{y}}_n = \begin{bmatrix} y_{n,1}(t_1) & \cdots & y_{n,1}(t_{N_t}) & \cdots & y_{n,N_y}(t_1) & \cdots & y_{n,N_y}(t_{N_t}) \end{bmatrix}^\top \tag{66}$$

$$\hat{\mathbf{f}}_{n-1/2} = \begin{bmatrix} \tilde{f}_{n-1/2,1}(t_1) & \cdots & \tilde{f}_{n-1/2,1}(t_{N_t}) & \cdots & \tilde{f}_{n-1/2,N_y}(t_1) & \cdots & \tilde{f}_{n-1/2,N_y}(t_{N_t}) \end{bmatrix}^\top \tag{67}$$

The inverse FFT can then be written as a linear operation

$$\hat{\mathbf{y}}_n = \mathcal{F}^- \mathbf{z}_n, \hat{\mathbf{f}}_{n-1/2} = \mathcal{F}^- \mathbf{b}_{n-1/2} \tag{68}$$

with the sparse operator

$$\mathcal{F}^- = \mathbf{I}_{N_y} \otimes \mathbf{Q}(\omega) \tag{69}$$

where $\mathbf{Q}(\omega)$ is the matrix of the time samples of trigonometrical functions

$$\mathbf{Q}(\omega) = \begin{bmatrix} \frac{1}{\sqrt{2}} & \sin\frac{\omega t_1}{\upsilon} & \cos\frac{\omega t_1}{\upsilon} & \cdots & \sin\frac{N_h \omega t_1}{\upsilon} & \cos\frac{N_h \omega t_1}{\upsilon} \\ \frac{1}{\sqrt{2}} & \sin\frac{\omega t_2}{\upsilon} & \cos\frac{\omega t_2}{\upsilon} & \cdots & \sin\frac{N_h \omega t_2}{\upsilon} & \cos\frac{N_h \omega t_2}{\upsilon} \\ \vdots & \vdots & \vdots & \ddots & \vdots & \vdots \\ \frac{1}{\sqrt{2}} & \sin\frac{\omega t_{N_t}}{\upsilon} & \cos\frac{\omega t_{N_t}}{\upsilon} & \cdots & \sin\frac{N_h \omega t_{N_t}}{\upsilon} & \cos\frac{N_h \omega t_{N_t}}{\upsilon} \end{bmatrix} \tag{70}$$

Similarly, the FFT to obtain the Fourier coefficients is written as

$$\mathbf{z}_n = \mathcal{F}^+ \hat{\mathbf{y}}_n, \mathbf{b}_{n-1/2} = \mathcal{F}^+ \hat{\mathbf{f}}_{n-1/2} \tag{71}$$

where the FFT operator is computed by $\mathcal{F}^+ = (\mathcal{F}^-)^\top \left[\mathcal{F}^-(\mathcal{F}^-)^\top\right]^{-1}$.

The Jacobian matrix of the residual function (63) with respect to $\mathbf{z}_{n-1}$ and $\mathbf{z}_n$ can be obtained as

$$\frac{\partial \mathbf{h}_{n-1/2}}{\partial \mathbf{z}_{n-1}} = \left(\bar{\mathbf{M}}_{n-1} \otimes \mathbf{\Theta} - \bar{\mathbf{K}}_{n-1/2} \otimes \mathbf{I}_{N_c}\right) + \frac{\partial \mathbf{b}_{n-1/2}}{\partial \mathbf{z}_{n-1}} \tag{72}$$

$$\frac{\partial \mathbf{h}_{n-1/2}}{\partial \mathbf{z}_n} = \left(\bar{\mathbf{M}}_n \otimes \mathbf{\Theta} + \bar{\mathbf{K}}_{n-1/2} \otimes \mathbf{I}_{N_c}\right) + \frac{\partial \mathbf{b}_{n-1/2}}{\partial \mathbf{z}_n} \tag{73}$$

The difficulty in evaluating the Jacobian matrix lies in the computation of $\partial \mathbf{b}_{n-1/2}/\partial \mathbf{z}_n$. This also requires the AFT technique. Noting that $\tilde{\mathbf{f}}_{n-1/2}$ is a function of both $\mathbf{y}_n$ and $\dot{\mathbf{y}}_n$ so that the Jacobian matrix computation needs to be written as

$$\begin{aligned} \frac{\partial \mathbf{b}_{n-1/2}}{\partial \mathbf{z}_n} &= \frac{\partial \mathbf{b}_{n-1/2}}{\partial \hat{\mathbf{f}}_{n-1/2}} \frac{\partial \hat{\mathbf{f}}_{n-1/2}}{\partial \mathbf{z}_n} = \mathcal{F}^+ \frac{\partial \hat{\mathbf{f}}_{n-1/2}}{\partial \mathbf{z}_n} \\ &= \mathcal{F}^+ \left(\frac{\partial \hat{\mathbf{f}}_{n-1/2}}{\partial \hat{\mathbf{y}}_n} \frac{\partial \hat{\mathbf{y}}_n}{\partial \mathbf{z}_n} + \frac{\partial \hat{\mathbf{f}}_{n-1/2}}{\partial \hat{\dot{\mathbf{y}}}_n} \frac{\partial \hat{\dot{\mathbf{y}}}_n}{\partial \mathbf{z}_n} \right) = \mathcal{F}^+ \frac{\partial \hat{\mathbf{f}}_{n-1/2}}{\partial \hat{\mathbf{y}}_n} \mathcal{F}^- + \mathcal{F}^+ \frac{\partial \hat{\mathbf{f}}_{n-1/2}}{\partial \hat{\dot{\mathbf{y}}}_n} \left\{ \mathbf{I}_{N_y} \otimes [\mathbf{Q}(\omega)\mathbf{\Theta}] \right\} \end{aligned} \tag{74}$$

Similar procedure is applicable for computing $\partial \mathbf{b}_{n-1/2}/\partial \mathbf{z}_{n-1}$. The same method is also applied for handling the boundary nodal equations (64) but it is noteworthy that the FFT operator for boundary equations is of size $N_c \times 3N_t$ here. From Eqs. (29-34) $\partial \tilde{\mathbf{f}}_{n-1/2}/\partial \mathbf{y}_n$ and $\partial \tilde{\mathbf{f}}_{n-1/2}/\partial \dot{\mathbf{y}}_n$ can be derived analytically (see Appendix B), which are then evaluated at the sampled time instances in a period and further rearranged to obtain $\partial \hat{\mathbf{f}}_{n-1/2}/\partial \hat{\mathbf{y}}_n$ and $\partial \hat{\mathbf{f}}_{n-1/2}/\partial \hat{\dot{\mathbf{y}}}_n$. Once the residual and Jacobian matrix are available, Newton's method can be used for iteration to solve the equation. In addition, for this two-point boundary valued problem spatially discretized using the first-order finite difference, only the two neigboring nodes are coupled and hence the problem can be solved from the fairlead node by node without assembling the global mass, stiffness matrices and the force vector. In iteration for solving the equations, the coefficient vector $\mathbf{z}_n$ for all the nodes are updated by

$$\mathbf{z}_n^{i+1} = \mathbf{z}_n^i + \gamma \Delta \mathbf{z}_n^i \tag{75}$$

where $\Delta\mathbf{z}_n^i$ is the state increment, γ is the relaxation factor which is in the range of 0 and 1 to slow the update, and i is the iteration step index. The adjustment method of the relaxation factor proposed in [16] is applied here.

The error is defined as [16]

$$e^i = \frac{1}{N_c N} \sum_{n=1}^{N} \sum_{j=1}^{N_c} \left|\Delta z_{n,j}^i\right| \tag{76}$$

3.3. Solving procedure

Providing the cable and environmental parameters and the cable static solution, the presented method can be used to conduct periodic responses analysis. Given the forced motion frequency, the FFT and inverse FFT operators can be prepared for use. The solving procedure is summarized as below.

i Evaluate $\bar{\mathbf{M}}_n$ and $\bar{\mathbf{K}}_n$ for $1 \le n \le N$ from the static solution using Eqs. (36,37);

ii Initialize $\mathbf{z}_n$ for all nodes;

iii Evaluate $\hat{\mathbf{y}}_n$ and $\hat{\dot{\mathbf{y}}}_n$ using the inverse FFT, Eq. (68), and rearrange the vector to obtain $\mathbf{y}_n(t_j)$ and $\dot{\mathbf{y}}_n(t_j)$ for all nodes and time instances;

iv Evaluate $\tilde{\mathbf{M}}_n$, $\tilde{\mathbf{K}}_n$ and $\mathbf{f}_n$ for all nodes using Eqs. (38,29–34);

v Evaluate $\tilde{\mathbf{f}}_{n-1/2}$, $\partial\tilde{\mathbf{f}}_{n-1/2}/\partial\mathbf{y}_n$, $\partial\tilde{\mathbf{f}}_{n-1/2}/\partial\mathbf{y}_{n-1}$, $\tilde{\mathbf{f}}_{n-1/2}/\partial\dot{\mathbf{y}}_n$ and $\tilde{\mathbf{f}}_{n-1/2}/\partial\dot{\mathbf{y}}_{n-1}$ using Eq. (40) and for boundary nodes using Eqs. (42-45);

vi Rearrange $\tilde{\mathbf{f}}_{n-1/2}$ for all nodes and time instances to obtain $\hat{\mathbf{f}}_{n-1/2}$ and rearrange $\tilde{\mathbf{f}}_{n-1/2}/\partial\mathbf{y}_n$ and $\tilde{\mathbf{f}}_{n-1/2}/\partial\mathbf{y}_{n-1}$ to obtain $\hat{\mathbf{f}}_{n-1/2}/\partial\hat{\mathbf{y}}_n$, $\hat{\mathbf{f}}_{n-1/2}/\partial\hat{\mathbf{y}}_{n-1}$, $\hat{\mathbf{f}}_{n-1/2}/\partial\hat{\dot{\mathbf{y}}}_{n-1}$ and $\hat{\mathbf{f}}_{n-1/2}/\partial\hat{\dot{\mathbf{y}}}_{n-1}$;

vii Obtain $\mathbf{h}_{n-1/2}$ using Eq. (63) and $\mathbf{h}_1$ and $\mathbf{h}_N$ using Eq. (64) and $\partial\mathbf{h}_{n-1/2}/\partial\mathbf{z}_n$ and $\partial\mathbf{h}_{n-1/2}/\partial\mathbf{z}_n$ using Eqs. (72,73) with the FFT and inverse FFT operators;

viii Solve $\Delta\mathbf{z}_n$ and evaluate the error and update $\mathbf{z}_n$ using Eq. (75);

ix Check the error using Eq. (76) and repeat steps 3-8 before convergence.

x Stop if convergence is achieved or the maximum number of iterations is reached.

The method is implemented in C++ with Eigen library [48] for handling linear algebra, matrix and vector operations.

4. Application and discussion

In this section, a typical mooring cable is analyzed using the presented method and the results are compared with corresponding time-domain analysis results. The open-source mooring system simulation program developed by the authors, named OpenMOOR, which has been verified and applied in [7, 49], is used for the time-domain analysis. The generalized-α method is used for time stepping [50].

4.1. Description of the simulated mooring cable

The mooring cable of the OC3 Hywind platform for the spar-type floating offshore wind turbine is used [51, 52]. The cable properties are listed in Table 1 along with the hydrodynamic coefficients which are adopted following [5]. In the following numerical analyses, to focus on the multi-HB method, the cable is considered to be in still water and the seabed interaction is ignored here. In this case, the constant terms in the Fourier expansion, i.e. Eqs. (49,50), are omitted. Hence $N_c = 2N_h$ and correspondingly the first column of the matrix $\mathbf{Q}(\omega)$ in Eq. (70) is also eliminated.

The cable static profile is shown in Fig. 2 which is solved using a shooting procedure [15]. The cable is divided into 49 segments with 50 nodes. For a fair comparison of the computation efficiency, in using the time-domain method, the static solution is used as the starting point. In harmonic balance analysis, the static solution is used along with zero dynamic responses as initial guess, i.e. $\mathbf{z}_n = \mathbf{0}$.

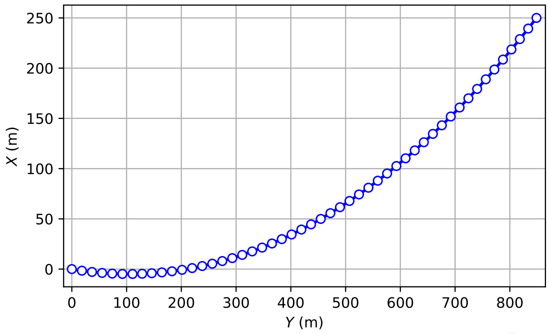

Figure 2: Static profile of the simulated cable (circles indicate the node position).

Table 1: Cable properties and environmental parameters

Parameter	Symbol	Unit	Value
Diameter	d	m	0.09
Unstretched length	L_0	m	902.2
Mass per unit length	m	kg/m	77.7066
Submerged weight per unit length	w_0	N/m	698.094
Elastic stiffness	EA	N	3.84243E8
Static cable depth	h	m	250
Static cable radius	l	m	848.67
Added mass coefficient	C_a	-	1.0
Drag coefficient	C_{dt}, C_{dn}, C_{db}	-	0, 1.6, 1.6

4.2. Convergence of the multi-HB method

The convergence of the presented method is first studied. The cable is forced with harmonic motions at the fairlead in the Y direction (surge motion). The frequency is considered to be 0.05 Hz when the non-linearity effect can be clearly seen in the following results. In using the multi-HB method, the integer $\nu = 1$ is adopted since no sub-harmonic responses have been observed in this case; the initial relaxation factor is set to be 1.0, and the convergence tolerance is considered to be 10^{-10}. The first case considers the amplitude of the fairlead displacement to be 5.0 m and in a second case, the amplitude is increased to 9.0 m. The error evolution with respect to the iteration step is plotted in Fig. 3 and the obtained cable tensions, $EA\varepsilon$, at the fairlead are plotted in Fig. 4. Results solved using different values of the harmonic balance parameters are presented for comparison.

It can be seen from Fig. 3 that for all the cases, the computation is able to achieve a fast convergence within ten steps. Generally, more iterations are required when higher-order harmonics are included and a larger number of time points are used. More importantly, even for the difficult case when cable tension becomes non-positive during the cable motion, which is known as an ill-posed problem for perfectly flexible cables [53], convergence can still be achieved with the multi-HB method, as shown in Fig. 4 for the case when the forced motion has an amplitude of 9.0 m and the fairlead tension is zero around $t = 15$ s. This is because the Jacobian matrix of the multi-HB method is constructed from all the time instances in one period and therefore it is nonsingular even if the Jacobian matrix of the time-domain equation is singular for some time instances. In Fig. 4, by comparing the results obtained using 9 harmonics and more, it can be concluded that the solution is converged with 9 harmonics in these two cases. Actually, with 3 harmonics the method can already achieve a quite high accuracy as compared to those obtained using 9 harmonics.

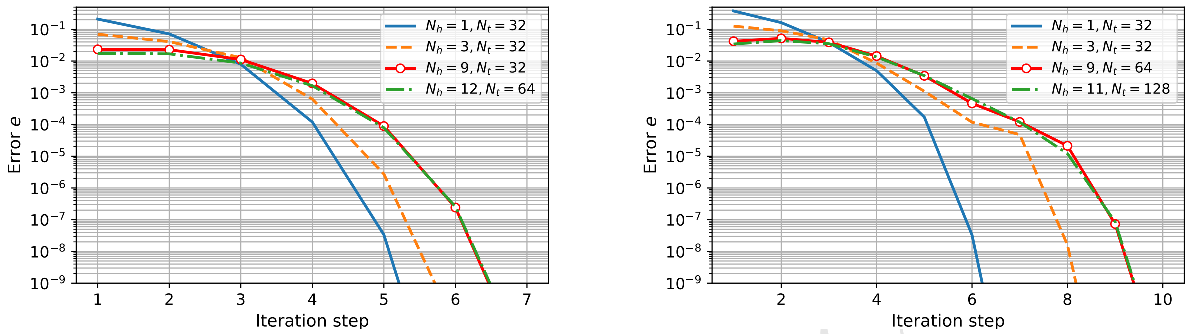

Figure 3: Error evolution in the multi-HB analysis (left) forced fairlead motion in Y direction of amplitude 5.0 m; (right) forced fairlead motion in Y direction of amplitude 9.0 m.

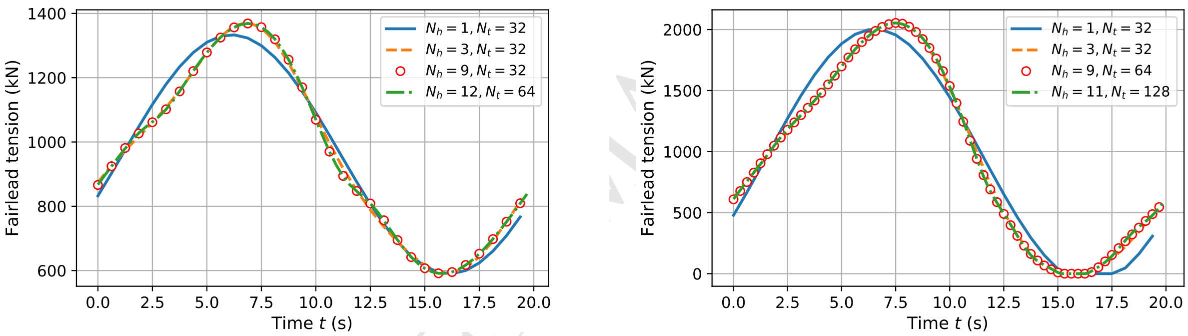

Figure 4: Fairlead tensions solved using the multi-HB method (left) forced fairlead motion in Y direction of amplitude 5.0 m; (right) forced fairlead motion in Y direction of amplitude 9.0 m.

4.3. Comparison of time- and frequency-domain methods

To verify the presented method and to show its advantages, simulations are carried out with the comparison to the time-domain method. As shown in the preceding section, $N_h = 9$ and $N_t = 32$ are sufficient for the convergence of the multi-HB analysis and they are thus adopted in the following analysis. In using the time-domain method, the convergence tolerance is also set to be 10^{-10}. Time domain analyses commonly start with the static solution with zero displacements and zero velocity, and hence some time is required to dissipate the transient responses so that the cable motion can reach the steady state. In the analysis, the displacement is ramped to the target value in half of a period and therefore at least two periods are required. The time needed for the transient responses to dying out depends on the system damping. For mooring cables, due to the hydrodynamic drag effect, several periods may be sufficient. As shown in Fig. 5, with the transverse drag coefficient of 1.6 in Table 1, the solution reaches the steady state in 3 periods, while decreasing the drag coefficient to 0.1, at least four periods are required. The accuracy and computational efficiency also depend on the time step, a test shows that a time step of 0.1 s is the minimum step to prevent the numerical drift of the cable displacement at the fairlead which is a known issue of this finite difference cable modal [16]. In the following, the time step is considered to be 0.1 s and the time-domain analysis is performed for three periods of the forced motion. The cable responses in the third period are assumed to be the steady responses to be compared with the harmonic balance analysis results.

Four cases are studied for comparison. In the first three cases, a forced motion of a displacement amplitude of 5.0 m and frequency of 0.05 Hz is considered respectively in Y, X, and Z directions. In the last case, the forced motion is considered in both Y and Z directions: the motion in the Y direction has a displacement amplitude of 2.5 m and frequency of 0.1 Hz and the motion in the Z direction is of a displacement amplitude of 5.0 m and a frequency of 0.05 Hz. The computation times to obtain the steady-state response using the time-domain method and the multi-HB method are compared in Table 2. Note that the value listed for the time-domain method is the time taken to complete a three-period simulation. The computations were performed on a 16-core Windows desktop (Intel i7-8700 CPU @ 3.20 GHz). It is seen that the multi-HB method is much efficient and the computational time is almost equivalent to the time needed to run the time-domain method for one period. Additionally, for such a nonlinear system, the time required for the system to reach the steady state is not known beforehand and for systems with less damping, more time is required as shown in Fig. 5.

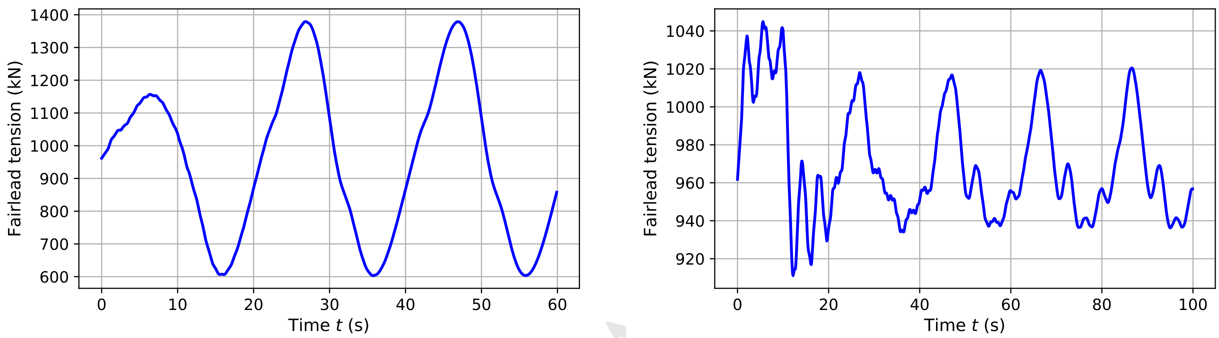

Figure 5: Fairlead tension time history solved using the time domain method (left) with hydrodynamic drag coefficients $C_{dt} = 0$ and $C_{dn} = C_{db} = 1.6$; (right) with hydrodynamic drag coefficients $C_{dt} = 0$ and $C_{dn} = C_{db} = 0.1$.

Table 2: Computational efficiency comparison

Case no.	Time-domain computation (s)	Multi-HB computation (s)	Description
1	6.03	1.40	motion in Y direction
2	6.07	1.40	motion in X direction
3	6.47	2.43	motion in Z direction
4	6.74	3.01	motion in both Y and Z direction

The cable responses solved using the time-domain method and the multi-HB are compared in Figs. 6–9 where the fairlead tension and the nodal solution corresponding to the 25th node (with $s = 441.11$ m) are plotted. In most of the graphics, results obtained using the two methods are found to be pretty consistent. Relatively observable differences are seen in the fairlead tension and the nodal strain of Fig. 8 when the forced motion is in the out-of-plane direction. This is because the overall tension/strain variation is small since the forced motion is in the out-of-plane. Besides, the super-harmonic responses are clearly captured in the cable tension, as also reported in the numerical study using time domain methods by [54].

The numerical results clearly demonstrate that in the analyzed cases, the multi-HB method has achieved comparable accuracy as the time-domain analysis while it is more efficient. In addition, as seen from the solving procedure given in Section 3.3, the AFT technique requires the FFT and inverse FFT operations for all nodes which can be done in parallel for further improving the computational efficiency. To summarize, the multi-HB method is found to be advantageous for periodic analyses of mooring cables.

5. Conclusion

This study has proposed and formulated a multi-HB method for a three-dimensional mooring cable under periodic fairlead motion. The governing equations of the cable are first represented in an incremental form and then spatially discretized using the finite difference method. The nodal equations are transformed into the frequency domain by

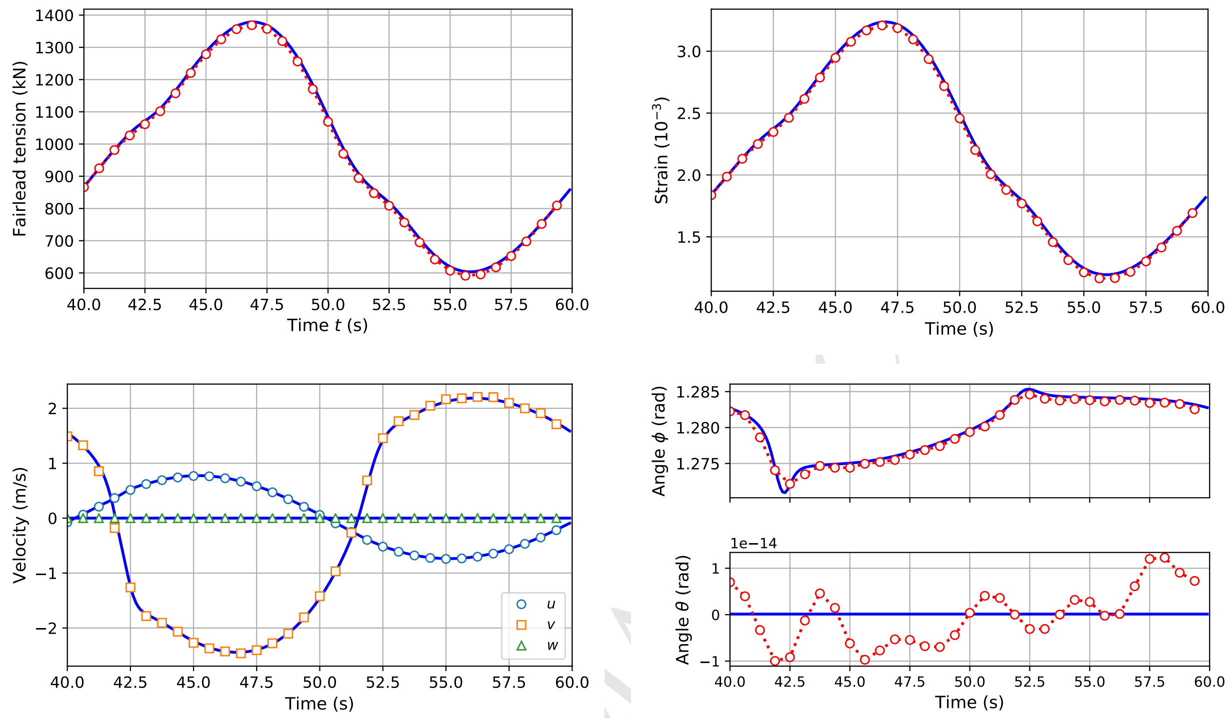

Figure 6: Comparison of the fairlead tension and nodal solution corresponding to the 25th node with s = 441.11 m when the forced motion is in Y direction. Lines correspond to the time-domain analysis results and symbols indicate the multi-HB analysis results.

Fourier expansion. The AFT technique is applied to handle the geometrical and hydrodynamic non-linearity accurately. The presented method is implemented and compared with a time domain method based on numerical studies of a typical mooring cable. The following conclusions can be drawn:

i The multi-HB method together with the AFT technique is promising to solve periodic mooring cable motion. It can handle the geometric and hydrodynamic nonlinearity and the case when cable tension becomes zero.

ii The multi-HB method is accurate and more efficient as compared to the time-domain method for analyzing the periodic cable responses.

iii The method is able to capture the super-harmonic cable responses and is promising for further parametric analyses of mooring cables.

Future studies will focus on local and global stability analysis of mooring cables with nonlinear hydrodynamics based on the presented method.

Acknowledgments

This work was partly supported by the Irish Research Council (IRC) via the Government of Ireland Postdoctoral Fellowship (Project ID: GOIPD/2017/1260) and the European Unions Horizon 2020 research and innovation programme under the Marie Skłodowska-Curie EID project ICONN Grant Agreement No. 675659, which is gratefully acknowledged.

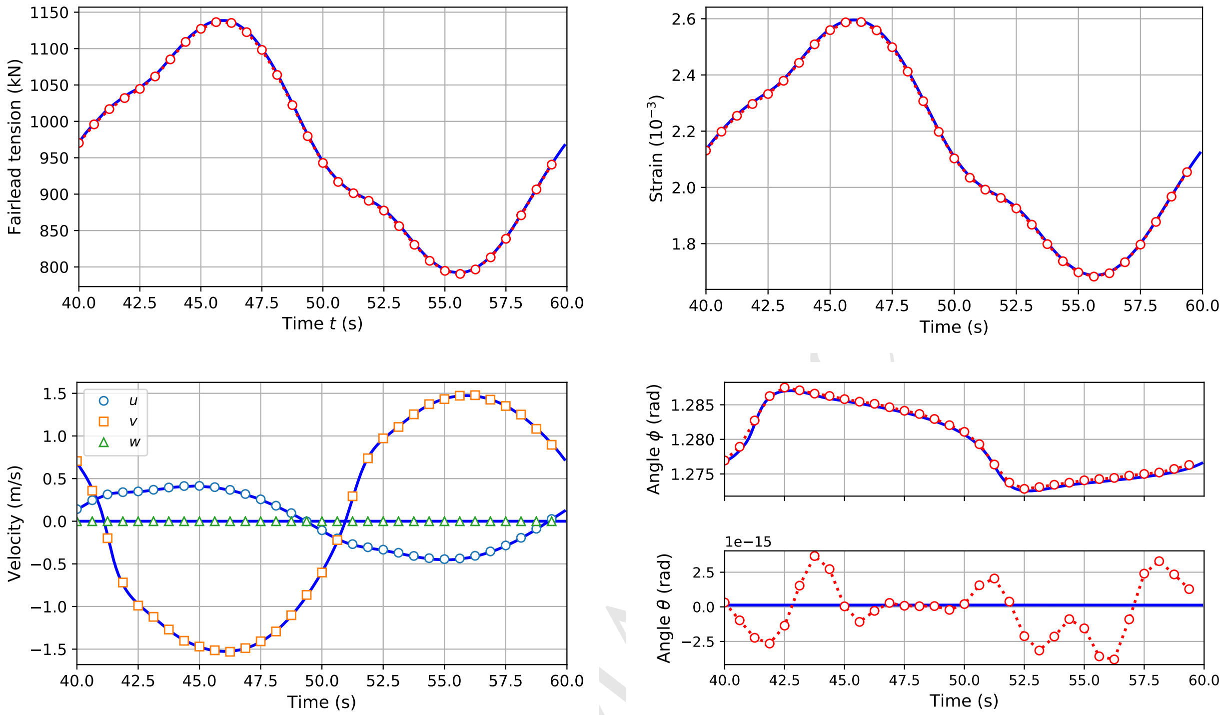

Figure 7: Comparison of the fairlead tension and nodal solution corresponding to the 25th node with s = 441.11 m when the forced motion is in X direction. Lines correspond to the time-domain analysis results and symbols indicate the multi-HB analysis results.

Appendix A. Kronecker product

The Kronecker product of two matrices is calculated by

$$\mathbf{A} \otimes \mathbf{E} = \begin{bmatrix} a_{11} & a_{12} & \cdots & a_{1q} \\ a_{21} & a_{22} & \cdots & a_{2q} \\ \vdots & \vdots & \ddots & \vdots \\ a_{p1} & a_{p2} & \cdots & a_{pq} \end{bmatrix} \otimes \mathbf{E} = \begin{bmatrix} a_{11}\mathbf{E} & a_{12}\mathbf{E} & \cdots & a_{1q}\mathbf{E} \\ a_{21}\mathbf{E} & a_{22}\mathbf{E} & \cdots & a_{2q}\mathbf{E} \\ \vdots & \vdots & \ddots & \vdots \\ a_{p1}\mathbf{E} & a_{p2}\mathbf{E} & \cdots & a_{pq}\mathbf{E} \end{bmatrix}$$

where $a_{(\cdot,\cdot)} \in \mathbb{R}$ is an element of matrix $\mathbf{A}$ $(p \times q)$.

Appendix B. Matrix differentiation

In the derivation of $\partial \tilde{\mathbf{f}}_{n-1/2}/\partial \mathbf{y}$, the following matrix differentiation expression is used

$$\frac{\partial \mathbf{M}(\mathbf{y})\mathbf{x}}{\partial \mathbf{y}} = \begin{bmatrix} \vdots \\ \mathbf{x}^\top \frac{\partial \mathbf{m}_p^\top}{\partial \mathbf{y}} \\ \vdots \end{bmatrix} \tag{B.1}$$

where $\mathbf{x}$ is a vector and $\mathbf{m}_p$ denotes the pth row of the $\mathbf{M}$ matrix.

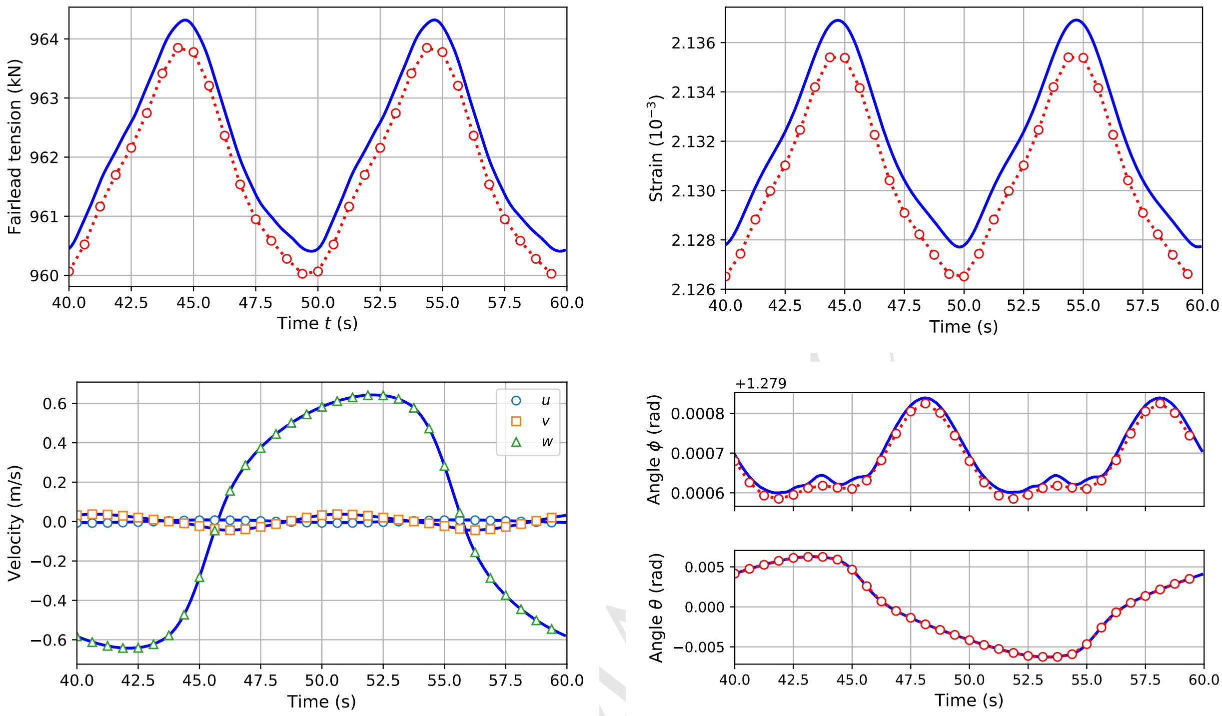

Figure 8: Comparison of the fairlead tension and nodal solution corresponding to the 25th node with s = 441.11 m when the forced motion is in Z direction. Lines correspond to the time-domain analysis results and symbols indicate the multi-HB analysis results.

References

[1] S. Butterfield, W. Musial, J. Jonkman, P. Sclavounos, L. Wayman, Engineering challenges for floating offshore wind turbines, in: Proc. of the 2005 Copenhagen Offshore Wind Conference, The European Wind Energy Association, 2005, pp. 377–382.

[2] D. Matha, M. Schlipf, R. Pereira, J. Jonkman, Challenges in simulation of aerodynamics, hydrodynamics, and mooring-line dynamics of floating offshore wind turbines, in: Proc. of the 21st Offshore and Polar Engineering Conference, International Society of Offshore and Polar Engineers, 2011.

[3] B. W. Kim, H. G. Sung, J. H. Kim, S. Y. Hong, Comparison of linear spring and nonlinear fem methods in dynamic coupled analysis of floating structure and mooring system, J. Fluids Struct. 42 (2013) 205–227. doi:10.1016/j.jfluidstructs.2013.07.002.

[4] M. Hall, B. Buckham, C. Crawford, Evaluating the importance of mooring line model fidelity in floating offshore wind turbine simulations, Wind Energy 17 (12) (2014) 1835–1853. doi:10.1002/we.1669.

[5] J. Azcona, D. Palacio, X. Munduate, L. González, T. A. Nygaard, Impact of mooring lines dynamics on the fatigue and ultimate loads of three offshore floating wind turbines computed with IEC 61400-3 guideline, Wind Energy 20 (5) (2017) 797–813. doi:10.1002/we.2064.

[6] J. E. Gutiérrez-Romero, J. García-Espinosa, B. Serván-Camas, B. Zamora-Parra, Non-linear dynamic analysis of the response of moored floating structures, Mar. Struct. 49 (2016) 116–137. doi:10.1016/j.marstruc.2016.05.002.

[7] L. Chen, B. Basu, S. R. K. Nielsen, A coupled finite difference mooring dynamics model for floating offshore wind turbine analysis, Ocean Eng. 162 (2018) 304–315. doi:10.1016/j.oceaneng.2018.05.001.

[8] B. Buckham, F. R. Driscoll, M. Nahon, Development of a finite element cable model for use in low-tension dynamics simulation, J. Appl. Mech. 71 (4) (2004) 476–485. doi:10.1115/1.1755691.

[9] Y. H. Bae, Development of a dynamic mooring module FEAM for FAST v8, Report, Texas A&M University (2014).

[10] E. Kreuzer, U. Wilke, Dynamics of mooring systems in ocean engineering, Archive Appl. Mech. 73 (3) (2003) 270–281. doi:10.1007/s00419-003-0288-3.

[11] M. Hall, A. Goupee, Validation of a lumped-mass mooring line model with DeepCwind semisubmersible model test data, Ocean Eng. 104 (2015) 590–603. doi:10.1016/j.oceaneng.2015.05.035.

[12] J. Azcona, X. Munduate, L. González, T. A. Nygaard, Experimental validation of a dynamic mooring lines code with tension and motion measurements of a submerged chain, Ocean Eng. 129 (2017) 415–427. doi:10.1016/j.oceaneng.2016.10.051.

[13] A. A. Tjavaras, The dynamics of highly extensible cables, Thesis, Massachusetts Institute of Technology (1996).

[14] A. A. Tjavaras, Q. Zhu, Y. Liu, M. S. Triantafyllou, D. K. P. Yue, The mechanics of highly-extensible cables, J. Sound Vib. 213 (4) (1998) 709–737. doi:10.1006/jsvi.1998.1526.

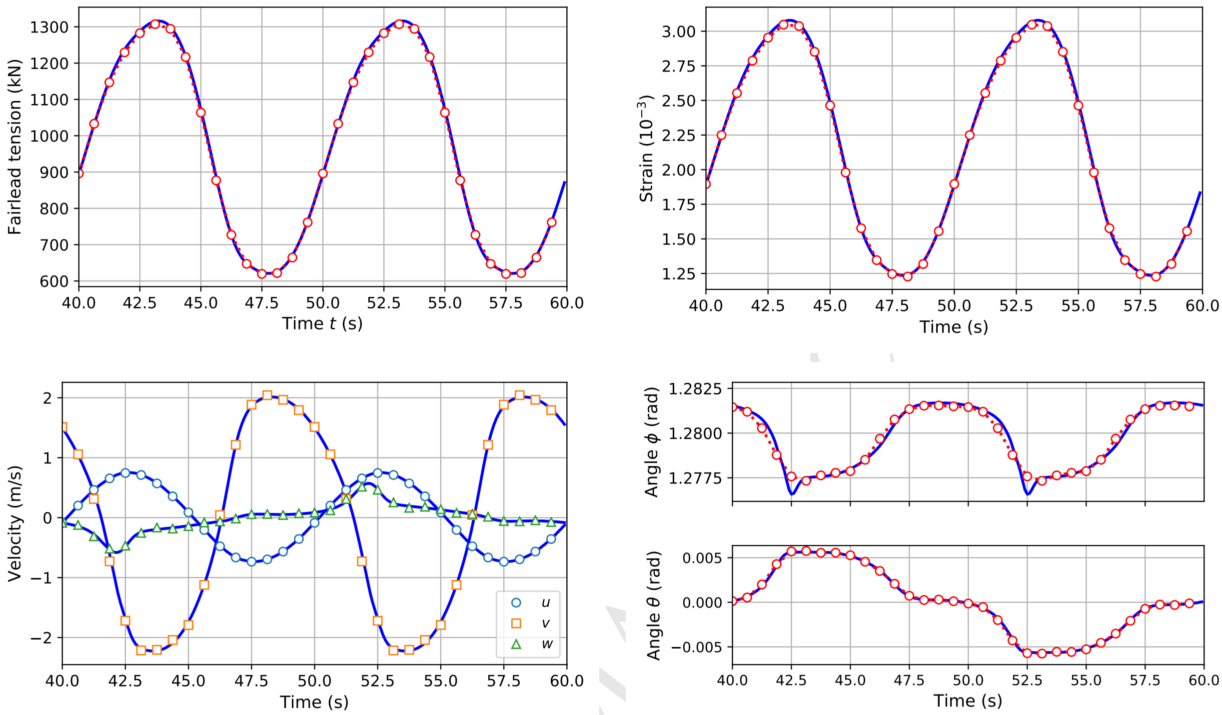

Figure 9: Comparison of the fairlead tension and nodal solution corresponding to the 25th node with s = 441.11 m when the forced motion is in both Y and Z directions. Lines correspond to the time-domain analysis results and symbols indicate the multi-HB analysis results.

[15] J. I. Gobat, The dynamics of geometrically compliant mooring systems, Thesis, Massachusetts Institute of Technology (2000).

[16] J. I. Gobat, M. A. Grosenbaugh, Time-domain numerical simulation of ocean cable structures, Ocean Eng. 33 (10) (2006) 1373–1400. doi:10.1016/j.oceaneng.2005.07.012.

[17] Y. Li, Q. Zhu, L. Liu, Y. Tang, Transient response of a spar-type floating offshore wind turbine with fractured mooring lines, Renew. Energy 122 (2018) 576–588. doi:10.1016/j.renene.2018.01.067.

[18] J. Davidson, J. V. Ringwood, Mathematical modelling of mooring systems for wave energy converters – A Review, Energies 10 (5) (2017) 666. doi:10.3390/en10050666.

[19] J. B. Thomsen, F. Ferri, J. P. Kofoed, Screening of available tools for dynamic mooring analysis of wave energy converters, Energies 10 (7) (2017) 853. doi:10.3390/en10070853.

[20] J. Palm, G. M. Paredes, C. Eskilsson, F. T. Pinto, L. Bergdahl, Simulation of mooring cable dynamics using a discontinuous Galerkin method, in: Proceedings of 5th International Conference on Computational Methods in Marine Engineering, 2013, pp. 1–12.

[21] J. Palm, C. Eskilsson, L. Bergdahl, An *hp*-adaptive discontinuous galerkin method for modelling snap loads in mooring cables, Ocean Eng. 144 (2017) 266–276. doi:10.1016/j.oceaneng.2017.08.041.

[22] R. Antonutti, C. Peyrard, A. Incecik, D. Ingram, L. Johanning, Dynamic mooring simulation with code_aster with application to a floating wind turbine, Ocean Eng. 151 (2018) 366–377. doi:10.1016/j.oceaneng.2017.11.018.

[23] F. S. Hover, Methods for positioning deeply-towed underwater cables, Thesis, Massachusetts Institute of Technology (1993).

[24] F. S. Hover, M. A. Grosenbaugh, M. S. Triantafyllou, Calculation of dynamic motions and tensions in towed underwater cables, IEEE J. Oceanic Eng. 19 (3) (1994) 449–457. doi:10.1109/48.312921.

[25] A. Sarkar, R. Eatock Taylor, Dynamics of mooring cables in random seas, J. Fluids Struct. 16 (2) (2002) 193–212. doi:10.1006/jfls.2001.0415.

[26] Y. Liu, L. Bergdahl, Frequency-domain dynamic analysis of cables, Eng. Struct. 19 (6) (1997) 499–506. doi:10.1016/S0141-0296(96)00091-0.

[27] I. K. Chatjigeorgiou, Second-order nonlinear dynamics of catenary pipelines: A frequency domain approach, Comput. Struct. 123 (2013) 1–14. doi:10.1016/j.compstruc.2013.04.006.

[28] N. M. Krylov, N. N. Bogoliubov, Introduction to non-linear mechanics, Vol. 11, Princeton University Press, 1943.

[29] W. J. Cunningham, Introduction to non-linear analysis, McGraw-Hill, 1958.

[30] M. Urabe, Galerkin's procedure for nonlinear periodic systems, Archive Ration. Mech. Anal. 20 (2) (1965) 120–152. doi:10.1007/BF00284614.

[31] F. H. Ling, X. X. Wu, Fast Galerkin method and its application to determine periodic solutions of non-linear oscillators, Int. J. Non-Linear

Mech. 22 (2) (1987) 89–98. doi:10.1016/0020-7462(87)90012-6.
[32] T. M. Cameron, J. H. Griffin, An alternating frequency/time domain method for calculating the steady-state response of nonlinear dynamic systems, J. Appl. Mech. 56 (1) (1989) 149–154. doi:10.1115/1.3176036.
[33] A. Cardona, T. Coune, A. Lerusse, M. Geradin, A multiharmonic method for non-linear vibration analysis, Int. J. Numer. Methods Eng. 37 (9) (1994) 1593–1608. doi:10.1002/nme.1620370911.
[34] J. P. Miralles, P. J. Jiménez Olivo, D. G. Peiró, G. V. Martín, J. M.-C. González, A fast Galerkin method to obtain the periodic solutions of a nonlinear oscillator, Appl. Math. Comput. 86 (23) (1997) 261–282. doi:10.1016/S0096-3003(96)00193-2.
[35] G. Kerschen, M. Peeters, J.-C. Golinval, A. F. Vakakis, Nonlinear normal modes, Part I: A useful framework for the structural dynamicist, Mech. Syst. Signal Proc. 23 (1) (2009) 170–194. doi:10.1016/j.ymssp.2008.04.002.
[36] M. Peeters, R. Viguié, G. Sérandour, G. Kerschen, J. C. Golinval, Nonlinear normal modes, Part II: Toward a practical computation using numerical continuation techniques, Mech. Syst. Signal Proc. 23 (1) (2009) 195–216. doi:10.1016/j.ymssp.2008.04.003.
[37] T. Detroux, L. Renson, G. Kerschen, The harmonic balance method for advanced analysis and design of nonlinear mechanical systems, in: Nonlinear Dynamics, Volume 2, Springer, 2014, pp. 19–34.
[38] L. Sun, L. Chen, Periodic responses of a taut cable attached with a friction damper computed using multi-harmonic balance method, in: Proc. IABSE Guangzhou 2016, IABSE, Zurich, Switzerland, 2016, pp. 464–471. doi:10.2749/222137816819258771.
[39] L. Chen, L. Sun, Steady-state analysis of cable with nonlinear damper via harmonic balance method for maximizing damping, J. Struct. Eng. 143 (2) (2017) 04016172. doi:10.1061/(ASCE)ST.1943-541X.0001645.
[40] L. Sun, L. Chen, Residual mode correction in calibrating nonlinear damper for vibration control of flexible structures, J. Sound Vib. 406 (2017) 197–207. doi:10.1016/j.jsv.2017.06.015.
[41] Y. Ni, G. Zheng, J. Ko, Nonlinear periodically forced vibration of stay cables, Trans. ASME J. Vib. Acoust. 126 (2) (2004) 245–252. doi:10.1115/1.1641800.
[42] M. Krack, L. Panning-von Scheidt, J. Wallaschek, A method for nonlinear modal analysis and synthesis: Application to harmonically forced and self-excited mechanical systems, J. Sound Vib. 332 (25) (2013) 6798–6814. doi:10.1016/j.jsv.2013.08.009.
[43] J. P. Breslin, Dynamic forces exerted by oscillating cables, J. Hydronaut. 8 (1) (1974) 19–31. doi:10.2514/3.62972.
[44] A. Bliek, Dynamic analysis of single span cables, Thesis, Massachusetts Institute of Technology (1984).
[45] J. R. Morison, J. W. Johnson, S. A. Schaaf, The force exerted by surface waves on piles, J. Petroleum Technol. 2 (05) (1950) 149–154. doi:10.2118/950149-G.
[46] W. H. Press, S. A. Teukolsky, W. T. Vetterling, B. P. Flannery, Numerical Recipes in C: The art of scientific computing Second Edition, Cambridge University Press, 2007.
[47] T. Detroux, L. Renson, L. Masset, G. Kerschen, The harmonic balance method for bifurcation analysis of large-scale nonlinear mechanical systems, Comput. Methods Appl. Mech. Eng. 296 (2015) 18–38. doi:10.1016/j.cma.2015.07.017.
[48] G. Guennebaud, B. Jacob, et al., Eigen v3, http://eigen.tuxfamily.org (2010).
[49] L. Chen, B. Basu, Fatigue load estimation of a spar-type floating offshore wind turbine considering wave-current interactions, Int. J. Fatigue (2018) (in press) doi:10.1016/j.ijfatigue.2018.06.002.
[50] J. Gobat, M. Grosenbaugh, Application of the generalized-α method to the time integration of the cable dynamics equations, Computer methods in applied mechanics and engineering 190 (37-38) (2001) 4817–4829. doi:10.1016/S0045-7825(00)00349-2.
[51] J. M. Jonkman, Definition of the floating system for phase IV of OC3, Report NREL/TP-500-47535, National Renewable Energy Laboratory (2010).
[52] J. M. Jonkman, D. Matha, Dynamics of offshore floating wind turbines–analysis of three concepts, Wind Energy 14 (4) (2011) 557–569. doi:10.1002/we.442.
[53] M. S. Triantafyllou, C. T. Howell, Dynamic response of cables under negative tension: an ill-posed problem, J. Sound Vib. 173 (4) (1994) 433–447. doi:10.1006/jsvi.1994.1239.
[54] L. Chen, B. Basu, A numerical study on super-harmonic responses of mooring cables subjected to top end excitations, in: International Symposium on the Dynamics and Aerodynamics of Cables (ISDAC2017), 2017, p. 291299.